HHS Public Access

Author manuscript

J Control Release. Author manuscript; available in PMC 2022 October 10.

Published in final edited form as:

J Control Release. 2021 October 10; 338: 773–783. doi:10.1016/j.jconrel.2021.09.013.

Release of basic fibroblast growth factor from acoustically-responsive scaffolds promotes therapeutic angiogenesis in the hind limb ischemia model

Hai Jin[1,2], **Carole Quesada**[2], **Mitra Aliabouzar**[2], **Oliver D. Kripfgans**[2,3,4], **Renny T. Franceschi**[3,5], **Jianhua Liu**[1], **Andrew J. Putnam**[3], **Mario L. Fabiilli**[2,3,4]

[1]Department of Medical Ultrasound, Guangzhou First People's Hospital, School of Medicine, South China University of Technology, Guangzhou, China

[2]Department of Radiology, University of Michigan, Ann Arbor, MI, USA

[3]Department of Biomedical Engineering, University of Michigan, Ann Arbor, MI, USA

[4]Applied Physics Program, University of Michigan, Ann Arbor, MI, USA

[5]Dental School, University of Michigan, Ann Arbor, MI, USA

Abstract

Pro-angiogenic growth factors have been studied as potential therapeutics for cardiovascular diseases like critical limb ischemia (CLI). However, the translation of these factors has remained a challenge, in part, due to problems associated with safe and effective delivery. Here, we describe a hydrogel-based delivery system for growth factors where release is modulated by focused ultrasound (FUS), specifically a mechanism termed acoustic droplet vaporization. With these fibrin-based, acoustically-responsive scaffolds (ARSs), release of a growth factor is non-invasively and spatiotemporally-controlled in an on-demand manner using non-thermal FUS. *In vitro* studies demonstrated sustained release of basic fibroblast growth factor (bFGF) from the ARSs using repeated applications of FUS. In *in vivo* studies, ARSs containing bFGF were implanted in mice following induction of hind limb ischemia, a preclinical model of CLI. During the 4-week study, mice in the ARS+FUS group longitudinally exhibited significantly more perfusion and less visible necrosis compared to other experimental groups. Additionally, significantly greater angiogenesis

Corresponding Author: Mario Fabiilli, Ph.D., University of Michigan, 1301 Catherine Street, 3226A Medical Sciences Building I, Ann Arbor, MI 48109-5667, Phone: 734-647-9326, mfabiill@umich.edu.

CRediT author statement

Hai Jin: Conceptualization, Methodology, Formal Analysis, Investigation, Writing – Original Draft, Writing – Review & Editing, Visualization, Funding Acquisition
Carole Quesada: Conceptualization, Investigation
Mitra Aliabouzar: Conceptualization, Investigation, Writing – Review & Editing
Oliver D. Kripfgans: Conceptualization, Methodology, Software, Writing – Review & Editing
Renny T. Franceschi: Conceptualization, Writing – Review & Editing
Jianhua Liu: Conceptualization, Writing – Review & Editing
Andrew J. Putnam: Conceptualization, Methodology, Writing – Review & Editing
Mario L. Fabiilli: Conceptualization, Methodology, Formal Analysis, Investigation, Resources, Writing – Original Draft, Writing – Review & Editing, Visualization, Supervision, Project Administration, Funding Acquisition

and less fibrosis were observed for the ARS+FUS group. Overall, these results highlight a promising, FUS-based method of delivering a pro-angiogenic growth factor for stimulating angiogenesis and reperfusion in a cardiovascular disease model. More broadly, these results could be used to personalize the delivery of therapeutics in different regenerative applications by actively controlling the release of a growth factor.

Keywords

hind limb ischemia; angiogenesis; ultrasound; drug delivery; fibrin; acoustic droplet vaporization; phase-shift emulsion; basic fibroblast growth factor

Introduction

Critical limb ischemia (CLI), an advanced stage of peripheral artery disease (PAD), is the third leading cause of atherosclerotic morbidity [1]. In CLI, arterial blockages reduce blood flow in the extremities, thus leading to chronic pain, numbness, limited mobility and tissue death. The gold standard in CLI treatment is surgical or endovascular revascularization. However, even with intervention, the prognosis for CLI patients is grim. Rates of restenosis can exceed 80% [2] and 29% of patients will either die or undergo a major amputation within one year of diagnosis [3]. Furthermore, 25% of CLI patients are ineligible for revascularization therapy because of existing co-morbidities [4]. Due to these limited options, experimental treatments have sought to improve tissue perfusion by stimulating the growth of new blood vessels to circumvent occluded vessels. One approach that has been evaluated in both preclinical [5–7] and clinical trials [8, 9] of PAD/CLI is the use of exogenous, pro-angiogenic growth factors (GFs) such as basic fibroblast growth factor (bFGF). However, conventional administration routes (e.g., intramuscular or intravascular injections) are ineffective for GFs, which have contributed to translational challenges [10].

Hydrogels are widely used within regenerative medicine to deliver GFs [11, 12]. These water-laden matrices have been shown to increase the *in vivo* half-life of GFs and facilitate angiogenesis. Release of a GF from a hydrogel is dominated by mechanisms like diffusion and matrix degradation [13]. As such, the ability to spatially and/or temporally control GF release from a conventional hydrogel is limited. Comparatively, endogenous pro-angiogenic GFs are expressed in spatiotemporally-regulated patterns during regeneration [14]. Upon implantation of a conventional hydrogel, the kinetics of GF release cannot be actively altered, which hinders the ability to personalize a GF therapy based on patient response.

We have developed a composite hydrogel that enables control of GF release using therapeutic, focused US (FUS). Globally, FUS is used clinically in both diagnostic and therapeutic applications [15]. FUS can be applied non-invasively, focused with sub-millimeter precision, and delivered in a spatiotemporally-defined manner to deeply located tissues. Our composite hydrogel, termed an acoustically-responsive scaffold (ARS), consists of a fibrin matrix containing a GF-loaded, phase-shift double emulsion (Figure 1A) [16, 17]. Fibrin, a component of the provisional matrix during wound healing, can facilitate angiogenesis and is approved by the United States Food and Drug Administration as a hemostatic agent [18]. Fibrin is enzymatically degraded within the body by plasmin

and matrix metalloproteinases [19]. The phase-shift double emulsion has a water-in-perfluorocarbon (PFC)-in-water (W_1/PFC/W_2) structure. A water-soluble payload, like a GF, is contained within the innermost W_1 phase. The PFC phase, which surrounds the W_1 droplets, is highly hydrophobic, thereby acting as a diffusion barrier for the encapsulated GF. PFCs, like perfluoro-*n*-alkanes, are used in biomedical applications since they are inert, non-metabolizable, and excreted via exhalation [20]. When exposed to FUS, the PFC phase is vaporized due to the tensile (i.e., rarefactional) part of the acoustic wave. This mechanism is known as acoustic droplet vaporization (ADV) and is a threshold-dependent process [21, 22]; thus ADV occurs when the applied acoustic pressure (P) is greater than the threshold pressure for ADV (P_{ADV}). The double emulsion morphology of the phase-shift emulsion is disrupted by ADV, which releases the encapsulated payload [23]. Thus, ADV enables on-demand release of a GF from an ARS.

Previously, FUS-modulated release of bFGF from an ARS stimulated endothelial network formation in an *in vitro* co-culture model [24]. Additionally, when ARSs were implanted subcutaneously, FUS-stimulated release of bFGF caused increases in angiogenesis and perfusion [25]. Spatial patterning of ADV in an ARS, and hence bFGF release, was also shown to elicit spatially-directed, host cell migration following *in vivo* implantation [26].

In prior studies, ARSs were implanted in non-ischemic tissues. Here, we investigate for the first time the impact of bFGF release from an ARS in a murine model of hind limb ischemia (HLI) [27] - a widely-used, preclinical model of CLI (Figure 1B). bFGF was encapsulated in a phase-shift double emulsion and subsequently incorporated within an ARS. The effect of single versus repeated FUS exposure on bFGF release was initially evaluated *in vitro*. Subsequently, ARSs were implanted in mice following induction of HLI and ischemia as well as perfusion were longitudinally monitored during the 28-day study. Angiogenesis, fibrosis, and macrophage infiltration were assessed using histological and immunohistochemical staining.

Materials and Methods

Preparation of phase-shift double emulsion

Phase-shift double emulsions containing perfluorooctane (C_8F_{18}, CAS#: 307-34-6, Alfa Aesar) were prepared using a microfluidic chip (Cat#: 3200146, junction: 14 × 17 μm, Dolomite, Royston, United Kingdom) as previously described [26]. The W_1 phase contained 3.6 mg/mL human recombinant bFGF (Cat#: GF003AF, EMD Millipore, Temecula, CA, USA). The double emulsion was characterized in the range of 1–30 μm using a Coulter Counter (Multisizer 4, Beckman Coulter, Brea, CA USA) with a 50 μm aperture. The average diameter, coefficient of variation, and concentration of the double emulsion (N=3 batches) were 5.8 ± 0.6 μm, 20.9 ± 7.4%, and (4.3 ± 0.8) × 10^9 droplets/mL, respectively.

Preparation of ARSs

A stock solution consisting of bovine fibrinogen (Sigma-Aldrich), reconstituted at 20 mg/mL clottable protein in Dulbecco's modified Eagle's medium (DMEM, Thermo Fisher Scientific, Waltham, MA, USA), and 0.1 U/mL bovine lung aprotinin (Sigma-Aldrich) was

degassed in a vacuum chamber. ARSs were prepared in custom, multi-well plates made by machining 9.5 mm diameter holes in a sheet of poly(methyl methacrylate) (85 mm × 125 mm × 5.5 mm). To create a well bottom, Tegaderm membrane (3M Healthcare, St. Paul, MN, USA) was adhered to the bottom of the sheet. ARSs (total volume = 0.25 mL, diameter = 9.5 mm, height = 3.5 mm) were generated by combining the fibrinogen solution, additional DMEM, bovine thrombin (Thrombin-JMI, Pfizer, NY, NY, USA), and emulsion. The final composition of the ARS was 10 mg/mL fibrinogen, 0.05 U/mL aprotinin, 2 U/mL thrombin, and 3.3% (v/v) emulsion. Each ARS nominally contained 10 μg bFGF. Fibrin scaffolds with 10 μg of unencapsulated bFGF (i.e., fibrin + bFGF) were prepared similarly. All scaffolds polymerized for 15 minutes at room temperature prior to subsequent handling.

FUS exposure

In vitro and *in vivo* FUS exposures were conducted in a tank filled with degassed, deionized water at 37°C. ADV was generated using a calibrated, focused, single-element transducer (H147, 2.5 MHz, f-number = 0.83, radius of curvature = 50 mm, −6 dB focal width: 0.51 mm, −6 dB focal length: 3.28 mm, Sonic Concepts, Inc., Bothell, WA USA). The transducer was connected to a computer-controlled, three-axis positioning system. Pulsed, acoustic waveforms were generated using a waveform generator (33500B, Agilent Technologies, Santa Clara, CA, USA) and a radiofrequency amplifier (GA-2500A Ritec Inc, Warwick, RI, USA). Tone bursts at 6.1 MPa peak rarefactional pressure, 5.4 μs pulse duration, and 100 Hz pulse repetition frequency were used. This peak rarefactional pressure (i.e., free field in water) was previously shown to be suprathreshold for ADV within the ARSs [29]. During FUS exposure, the transducer was rastered at 5 mm/s with a 0.5 mm lateral spacing between raster lines [29].

In vitro release of bFGF from ARSs

Following polymerization, the ARSs were aseptically transferred to a 24-well BioFlex plate (Flexcell International, Burlington, NC, USA). The well bottom of the BioFlex plate consists of a silicone elastomer membrane (thickness: ~0.25 mm) with an acoustic attenuation of 0.7 ± 0.2 dB/cm/MHz [30], which insignificantly attenuated the 2.5 MHz FUS. Each ARS was overlaid with 1 mL of media consisting of DMEM with 100 U/mL penicillin, 100 μg/mL streptomycin, and 2.5 μg/mL amphotericin B (Life Technologies). The total height of the volume within each well (i.e., ARS and media) was approximately 0.7 cm. The plate was placed in a standard tissue culture incubator (37°C, 5% carbon dioxide). The following day (i.e., day 1), the plate was positioned in the water tank such that only the bottom of the plate was in contact with the water. The FUS transducer was located beneath the plate and a subset of the ARSs were exposed to FUS at three axial planes 3 mm, 2 mm, and 1 mm above the well bottom. The overlying media was sampled on day 0 and within an hour after FUS exposure (i.e., day 1 and onward) by collecting 0.5 mL of the media and replacing the collected volume with 0.5 mL fresh media. The plate was returned to the incubator for the remainder of the experiment. For a subset of the ARSs, the FUS exposure was repeated every 3 days. ARSs that were not exposed to FUS served as controls. The overlying media was periodically sampled for all three groups during the 14-day experiment. Sink conditions were maintained throughout the experiment since the loading of bFGF in each ARS (i.e., 10 μg bFGF per 0.25 mL ARS with 1 mL overlying media) was lower than the bFGF

concentration in the W_1 phase of the emulsion (i.e., 3.6 mg/mL). Release of bFGF into the overlying media was quantified using an enzyme-linked immunosorbent assay (ELISA) (DY233, R&D System, Inc., Minneapolis, MN, USA) using a mass balance approach [28].

Implantation of ARSs in the HLI model

This *in vivo* research was conducted with the approval of the Institutional Animal Care & Use Committee (IACUC) at the University of Michigan. Female BALB/c mice (N=78, 57–70 days old, 20.4 ± 1.8 g, Charles River Laboratories, Wilmington, MA, USA) were acquired and housed for 4 weeks prior to use. Following anesthetization with isoflurane, the lower ventral hair on each mouse was removed by shaving and depilatory cream; the skin was subsequently disinfected with povidone-iodine. A skin incision was made in the left leg from the knee toward the medial thigh. Using silk suture (6–0, Ethicon, Somerville, NJ, USA), the proximal and distal ends of the femoral artery were ligated from the inguinal ligament to the bifurcation of the saphenous, genicular, and popliteal arteries, respectively. The femoral artery and its side branches between the ligatures were transected and excised. For experimental groups receiving implants, the hydrogel was placed at the site of femoral artery resection. In all cases, the wound was closed with interrupted nylon sutures (6–0, Ethicon). Based on B-mode ultrasound imaging (data not shown), each hydrogel was implanted at a depth of approximately 1.3–3 mm from the skin surface. Five experimental groups were interrogated: no intervention, FUS only, fibrin + bFGF, ARS, and ARS + FUS.

FUS was applied starting one day after induction of HLI (i.e., day 1) and repeated every 3 days during the study. Following anesthetization with isoflurane, each mouse was secured to a platform at the top of the water tank in a prone position. The mouse was positioned on the platform such that the upper left leg was within the exposure window (1.2 cm × 1.8 cm) of the platform (Figure 1B). The FUS transducer was positioned beneath the exposure window and FUS was applied across the entire exposure window at three axial planes located 3 mm, 2 mm, and 1 mm above the ventral surface of the mouse. The time required to complete the FUS exposure for each mouse was approximately 5 min. To account for any effects of repeated handling or anesthesia, groups not receiving FUS were exposed to sham FUS exposures.

Evaluation of ischemia

Ischemia was longitudinally scored in the left leg by modifying a semi-quantitative, visual scale [31]. The following 13-point scoring system was used: no necrosis or discoloration (13), 1 nail discoloration (12), ≥2 nail discoloration (11), 1 toe discoloration (10), ≥2 toe discoloration (9), foot discoloration (8), leg discoloration (7), 1 toe necrosis (6), ≥2 toe necrosis (5), necrosis in the anterior foot (4), necrosis in the posterior foot (3), necrosis in the lower leg (2), and necrosis in the upper leg (1). Mice that received a score of 1 were euthanized in accordance with our IACUC-approved protocol.

Evaluation of perfusion

Mice were anesthetized with isoflurane, placed in a supine position on a heated (i.e., 37°C) water blanket, and imaged with a PeriCam PSI HR (Perimed, Ardmore, PA USA) laser speckle contrast analysis (LASCA) system with Pimsoft software (Perimed). For each time

point, LASCA imaging was done prior to FUS exposure if both LASCA and FUS exposure were conducted on the same day. Image acquisition parameters were described previously [25]. Briefly, images were acquired at a rate of 0.096 images/s with a field of view of 2.0 × 2.8 cm. At each time point, the left leg, right leg, left foot, and right foot of each mouse were imaged. With the acquired images of the leg, the average relative perfusion was computed within four regions of interest (ROIs): adductor muscle, calf muscle, femoral artery, and saphenous artery. The average relative perfusion was also computed within an ROI encompassing the foot. For each of the five ROIs, a perfusion ratio was calculated by normalizing the average relative perfusion in a given ROI within the ischemic (i.e., left) leg or foot by the same corresponding ROI in the normal (i.e., right) leg or foot. To account for variations in the position of the leg between different groups and/or time points, the placement of ROIs within each leg was adjusted based on anatomical features of the leg.

Histological Analyses

Mice were euthanized on either day 14 or 28 post HLI surgery. Mice that were prematurely euthanized prior to their intended, experimental endpoints were excluded from histological analyses. Muscle tissues from the left upper leg (LUL), left lower leg (LLL), right upper leg (RUL), and right lower leg (RLL) were harvested, fixed overnight in aqueous buffered zinc formalin, and later embedded in paraffin. Tissue sections were immunohistochemically stained for CD31 (ab182981, Abcam, Cambridge, MA USA) and CD68 (ab125212, Abcam). Additionally, *in vitro* ARSs were fixed on day 14, sectioned, and stained for bFGF (ab92337, Abcam). Staining was visualized using a polymer-horseradish peroxidase conjugate (Envision+ System-HRP (DAB), Agilent, Santa Clara, CA USA). Sections were also stained with Masson's trichrome by the Tissue & Molecular Pathology Core at the University of Michigan.

Five fields of view per tissue section were acquired with an inverted microscope and a 20x objective (Eclipse Ti-E, Nikon, Melville, NY, USA). The densities of blood vessels, defined as CD31+ structures possessing a lumen, and macrophages, defined as punctate CD68+ structures, were determined in each stained section by at least two trained readers in a blinded manner. With Masson's trichrome staining, the area percent of the tissue that stained positive for collagen (i.e., blue) was determined using a custom macro in ImageJ (National Institutes of Health, Bethesda, MD, USA)

Statistics

Statistical analyses were performed in GraphPad Prism software (GraphPad Software, Inc., La Jolla, CA USA). For *in vitro* experiments, release data were fit to a first-order exponential model of solute diffusion in a highly porous gel [29, 32]. The following parameters from this model are reported: the percentage of bFGF released at infinite time (C_{max}) and rate constant (K). The 95% confidence intervals of C_{max} and K are shown as $S\,[S_L, S_H]$ where S is the average value, S_L is the lower bound value, and S_H is the upper bound value. In general, significant differences between groups were determined using a one-way ANOVA followed by Tukey's multiple comparisons test. Significant differences in survival were determined using a log-rank test of Kaplan-Meier curves.

Results

In vitro release of bFGF from ARSs

bFGF release from the ARSs was measured for 14 days (Figure 2A). Overall, release correlated with the number of times the ARSs were exposed to FUS. Significantly greater release was observed on day 1 for the two groups exposed to FUS versus the ARS control. For ARSs exposed to FUS every three days, significantly greater release was seen beginning on day 5, when compared to the group exposed to FUS only on day 1, at all matched time points. C_{max} was 5.8% [5.6, 6.1], 7.6% [7.4, 7.7], and 11.6% [10.9, 12.4] for the ARS, ARS + FUS (day 1), and ARS + FUS (every 3 days) groups, respectively. Multiple FUS exposures also yielded more extended release kinetics of bFGF; K was 1.8 day^{-1} [1.2, 3.1], 2.3 day^{-1} [1.9, 3.0], and 0.3 day^{-1} [0.2, 0.4] for the ARS, ARS + FUS (day 1), and ARS + FUS (every 3 days) groups, respectively.

Distinct morphological differences were observed in the ARSs in response to FUS exposure (Figure 2B). Qualitatively, the phase-shift emulsion in the ARS group appears more regularly shaped with a darker staining of bFGF. Comparatively, the emulsion in both +FUS groups demonstrated larger particles and a lighter staining for bFGF.

Improvement in Visual Ischemia

The left legs of the mice were longitudinally photographed during the study to enable visual score of ischemia (Figure 3A). Immediately after induction of HLI on day 0, the legs in all groups appeared discolored. For the no intervention, FUS, fibrin + bFGF, and ARS groups, discoloration persisted and necrosis was evident in some cases as early as days 6–7. For the ARS+FUS group, legs were still discolored at day 7, but qualitatively appeared more perfused than the other four groups. A noticeable improvement was seen in the ARS+FUS group beginning on days 10–14.

The ischemia scores for all groups are shown (Figure 3B). The ARS+FUS group displayed significantly greater scores (i.e., less ischemia) than the no intervention and FUS groups beginning on day 4, the fibrin + bFGF group beginning on day 7, and the ARS group beginning on day 10. The ARS+FUS group had higher scores compared to the other four groups from day 10 through day 28. Additionally, the ARS group exhibited significantly greater scores than the no intervention and FUS groups on day 7 and day 4, respectively.

Mice that displayed necrosis extending into the upper leg were euthanized prior to their intended, experimental endpoints (Supplemental Table 1). As such, Kaplan-Meier curves were generated for the five experimental groups (Figure 3C). A subset of mice in the no intervention, fibrin + bFGF, and ARS groups were euthanized prior to their intended endpoints; no mice were prematurely euthanized in the FUS and ARS+FUS groups. Losses were experienced between days 6 through 11. There were no significant differences among the survival curves ($p = 0.11$). Additionally, there were no significant differences in ischemia scores for no intervention, fibrin + bFGF, and ARSs groups when comparing scores for mice that reached the experimental endpoint versus all mice, including those that were prematurely euthanized (Supplemental Figure 1).

Enhancement of Perfusion

LASCA was used to monitor perfusion in the legs and feet of the mice (Figure 4A). Prior to surgery, the femoral and saphenous arteries were distinctly visible in the leg. Immediately after induction of HLI, there was a dramatic decrease in perfusion. Qualitatively, all groups displayed a longitudinal increase in perfusion during the experiment. The greatest differences were observed in the ARS+FUS group, which displayed an increase in diffuse LASCA signal surrounding the femoral and saphenous arteries.

The LASCA images were quantified by calculating the average signal intensity within four separate ROIs within the left (i.e., ischemic) leg - adductor muscle, calf muscle, femoral artery, and saphenous artery - as well as one ROI for the left foot and then normalizing by the average ROI intensity in the right (i.e., control) leg/foot (Figure 4B). Since HLI was generated based on the excision of the femoral artery, angiogenesis typically occurs within the lower leg and calf muscle [33]. Perfusion within the adductor muscle [34] and foot [35] are indicators of collateral flow (e.g., arteriogenesis) and total leg perfusion, respectively.

The perfusion ratio for the calf muscle is shown (Figure 4C). The ARS+FUS group displayed significantly higher perfusion than the fibrin + bFGF and ARS groups beginning on day 7. From day 14 though day 28, the ARS+FUS group exhibited significantly greater perfusion when compared to the other four experimental groups, with a maximum perfusion ratio of 149. Comparatively, the maximum perfusion ratio (i.e., after surgery) among the other four groups was 88. A ratio of 100 indicates equivalent perfusion in the left and right ROIs. With the other four ROIs, all groups exhibited longitudinal increases in perfusion, though there were no sustained significant differences in perfusion (Supplemental Figure 2). Additionally, there were no significant differences in perfusion for no intervention, fibrin + bFGF, and ARSs groups when comparing mice that reached the intended, experimental endpoint versus all mice, including those that were prematurely euthanized (Supplemental Figure 3).

Increased Angiogenesis

Blood vessel density was quantified in muscle tissue harvested on day 14 and day 28 using CD31 immunohistochemistry (Supplemental Figure 4A and Figure 5). On day 14, there was significantly greater angiogenesis in the LLL for the ARS+FUS group compared to the four experimental groups (i.e., 2.6 to 7.2-fold higher) as well as intact mice without HLI surgery (i.e., 7.7-fold higher) (Figure 5A and Figure 5B). On day 28, there was significantly greater angiogenesis in the LLL and RLL for the ARS+FUS group compared to the four experimental (i.e., 3.6 to 4.6-fold higher in LLL; 2.5 to 4.2-fold higher in the LUL) and control (i.e., 13.1- and 5.9-fold higher in the LLL and LUL, respectively) groups (Figure 5C and Figure 5D). With the ARS+FUS group, there was significantly more (i.e., 2.5-fold) blood vessels in the LLL versus LUL on day 28; this difference was not significant on day 14. Overall, with the exception of the no surgery group, greater vessel densities were seen in the left leg compared to the right leg.

Decreased Levels of Fibrosis

Muscle sections from the LLL and LUL were stained with Masson's trichrome (Figure 6A) and quantified for the area percent of the tissue staining positive for collagen (i.e., blue) (Figure 6B). With intact mice (i.e., no surgery group), collagen staining was mainly present around blood vessels. In the experimental groups, more diffuse collagen staining was observed within the muscle fibers, which was an indication of fibrosis. The no intervention, FUS, fibrin + bFGF, and ARS groups displayed significantly greater collagen areas compared to control mice in both the LLL and LUL groups. The ARS+FUS group was not significantly different than control mice in both the LLL and LUL. There were no significant differences when comparing LLL versus LUL among any of the groups.

Macrophage Infiltration

The density of macrophages was quantified in muscle harvested on day 28 using CD68 immunochemistry (Supplemental Figure 4B and Figure 7). Overall, there was a greater density of macrophages in the left leg compared to the right leg. There was a significantly higher density of CD68+ cells in the LLL versus LUL for the no intervention, FUS, and ARS+FUS groups. Additionally, a greater density was observed in the LLL of the ARS+FUS group compared to the four other groups.

Discussion

Multiple, suprathreshold FUS exposures triggered release of bFGF from ARSs implanted in the HLI model, which led to significantly greater perfusion in the calf muscle, angiogenesis, and recruitment of macrophages as well as less visible ischemia and fibrosis. Overall, these results are consistent with previous studies using the HLI model that showed an inverse correlation between therapeutic efficacy (e.g., angiogenesis, perfusion) and muscle fibrosis [36, 37] as well as infiltration of macrophages within the ischemic hind limb [38, 39]. As seen in the *in vitro* experiments, FUS exposures applied every three days yielded greater and more sustained release of bFGF from ARSs compared to a single FUS exposure or ARSs without FUS exposure. With ARSs, non-selective payload release (i.e., in the absence of FUS) correlated inversely with the molecular weight of the PFC in the phase-shift emulsion [29]. Similar to a previous study [26], a single FUS exposure yielded a burst release of payload from an ARS containing a perfluorooctane emulsion. The high boiling point of perfluorooctane (i.e., 100°C) prevented formation of gas bubbles that were stable after ADV at 37°C [28], which contributed to the faster release kinetics [29]. Here, repeated applications of FUS every three days enabled more extended release of bFGF. With a dextran payload, greater release was observed from ARSs with perfluorooctane emulsion when exposed to FUS at three axial planes versus a single plane on one day [29]. In previous microscopy-based studies with a fluorescent payload, a fraction of the encapsulated payload within each perfluorooctane droplet was released each time ADV disrupted the droplet morphology [28]. Consistent with bFGF staining in the *in vitro* ARSs, the high loading of emulsion within the ARS (i.e., 3.3% (v/v)), and hence close inter-droplet spacing, also facilitated coalescence of droplets during ADV/recondensation, as also observed previously [40]. In contrast, ADV generates stable gas bubbles in ARSs with phase-shift emulsions containing lower bulk boiling point PFCs [17]; this enables complete payload release from

a droplet in response to a single suprathreshold FUS exposure. However, the generation of stable gas bubbles within an ARS can lead to acoustic shadowing [26], thereby inhibiting subsequent FUS-based interactions with the ARS.

Despite having equivalent doses of bFGF, significantly greater therapeutic efficacy was observed with the ARS+FUS group compared to the ARS and fibrin+bFGF groups. In this study, each implant with bFGF contained 10 μg bFGF; comparatively, other studies investigating the therapeutic effect of bFGF delivery in the murine HLI model used doses of 25 μg [6, 7]. Overall, it has been shown that the microenvironmental concentration of a pro-angiogenic factor, and not the total dose, is critical for blood vessel growth [41]. With the ARS group, more of the bFGF payload was retained within the phase-shift emulsion given the lack of FUS exposure. Release of bFGF from a fibrin hydrogel exhibits a burst release profile dependent on fibrin density as well as the concentrations of thrombin and heparin [5], the latter of which is attributed to bFGF binding to fibrinogen via heparin-binding domains [42]. Previously, we measured a K of 0.9–1.1 day^{-1} for bFGF release from a fibrin scaffold [24]. Comparatively, K was 3 to 3.7-fold lower for ARS+FUS. Thus, extended release of bFGF likely contributed to therapeutic efficacy, as demonstrated with bFGF released from heparin-conjugated fibrin [6] and heparin-conjugated, poly(lactic-co-glycolic acid) (PLGA) nanoparticles in fibrin [7]. Consistent with these and another study [5], our results demonstrate increased angiogenesis and decreased fibrosis at day 28 in response to treatment with bFGF. Significant increases in perfusion were observed beginning on day 7, which is similar to studies delivering vascular endothelial growth factor (VEGF) and insulin-like growth factor 1 (IGF-1) from alginate hydrogels [31].

The highest density of CD68+ macrophages were also observed in the ARS+FUS group, which is potentially due to bFGF acting as a chemotactic factor for macrophages [43], and as will be discussed subsequently, the potential of FUS to stimulate macrophage infiltration. CD68 is a pan-macrophage marker and thus does not enable differentiation of M1 and M2 macrophages. The long-term presence of M1 and M2 macrophages at the site of tissue damage has been associated with chronic inflammation and fibrosis, respectively [44]. In this study, the elevated level of macrophages in the ARS+FUS group did not correlate with fibrosis. Overall, the impact of the phenotypic spectrum of macrophages on angiogenesis and tissue regeneration is not fully understood and is an active area of research. M1 and M2a macrophages can secrete VEGF and PDGF-BB that stimulate endothelial sprouting and vessel maturation, respectively [45]. The shift from an M1 to an M2 phenotype can also enhance arteriogenesis [46].

In this study, application of FUS alone did not produce any significant impacts on therapeutic efficacy. However, previous studies have demonstrated therapeutic benefits of FUS in the HLI model. For example, low intensity continuous wave ultrasound (2 MHz, 0.05 W/cm^2 spatial average temporal average intensity (I_{SATA})) [47] and pulsed, focused ultrasound (1 MHz, 5.8 MPa peak rarefactional pressure, 1 ms pulse duration, and 5 Hz pulse repetition frequency) [48] increased limb perfusion, angiogenesis, and mRNA expression of vascular endothelial growth factor (VEGF) in Sprague-Dawley rats. In C57BL/6J mice, low intensity ultrasound (1 MHz, 0.3 W/cm^2) increased perfusion, angiogenesis, as well as expression of VEGF, hypoxia inducible factor-1α, endothelial nitric

oxide synthase (eNOS), and p-Akt [49]. In intact C3H mice, pulsed FUS (1 MHz, 50 ms pulse duration, 1 Hz pulse repetition frequency, 133 W/cm^2 I_{SATA}) applied to the leg muscle increased macrophage infiltration and expression of various cytokines (e.g., IL-1α, tumor necrosis factor α) and growth factors (e.g., FGF, VEGF) [50]. It is important to note that differences in animal model/strain [51], surgical variations in the HLI model [52], and ultrasound parameters [53] have significant impacts on observed bioeffects in cardiovascular models. Compared to C57BL/6J mice, BALB/c mice – which were used in this study - are more prone to ischemic injury due to the presence of fewer pre-existing collateral vessels [54]. The ability of ultrasound to produce mechanical and thermal effects is highly dependent on acoustic parameters (e.g., frequency, pressure/intensity, pulse duration, and duty cycle) [15]. In the current study, FUS parameters were chosen based on the threshold for ADV in the ARS and to minimize the potential for heating by using a low duty cycle (i.e., 0.054%).

FUS has been previously used in combination with vascular drug delivery agents or cells in the HLI model. In C57BL/6J mice, PLGA nanoparticles loaded with bFGF were co-administered in the saphenous artery with a microbubble-based contrast agent and then exposed to pulsed ultrasound at 1 MHz [55]. Significantly more nanoparticles were deposited in the endothelium and the interstitial space between muscle fibers when co-administered with microbubbles and FUS. This single time point delivery of bFGF (administered dose: 0.65 μg) increased the caliber and density of collateral arterioles compared to a group receiving control nanoparticles and ultrasound, though no impact was observed on microvessel density. Comparatively, the bFGF dose used in the current study was higher and enabled extravascular release of bFGF due to the placement of the ARS at the wound site. Microbubbles in combination with ultrasound (1.3 MHz, mechanical index: 1.3, 1.3 kHz pulse repetition frequency) increased perfusion in C57BL/6J mice for over a day due to local release of adenosine triphosphate [56]. In both aforementioned examples, acoustically-driven cavitation, which has also been observed in ARSs [57], was a key underlying mechanism. In C3H mice, the tropism of infused human mesenchymal stem cells to ischemic muscle increased when administered in conjunction with pulsed FUS (1 MHz, 10 ms pulse duration, 5 Hz pulse repetition frequency) due to upregulation of local chemoattractants [58].

There were some limitations to this study. First, the surgical technique used to induce HLI did not enable study of arteriogenesis, which can be enhanced by bFGF [59, 60]. Second, surgically-induced ischemia is pathophysiologically different than clinically-observed CLI. The former is induced acutely and as seen in the presented data, there is some observed reperfusion even without intervention; as such, interventions are often applied soon after induction of ischemia during surgically-induced inflammation [61]. The latter develops progressively over years and is strongly linked to many risk factors (e.g., diabetes) [10]. Thus, preclinical models that more closely reflect the clinical manifestation are needed to facilitate translation of new therapies [27]. Third, we did not interrogate a fibrin+bFGF+FUS group since *in vitro* data (not shown) suggested that FUS did not impact the release of bFGF from a fibrin implant (i.e., fibrin + bFGF). However as discussed previously, FUS can generate therapeutic effects in the HLI model, though typically at much higher duty cycles than used here. Fourth, we investigated the delivery of a single growth factor (i.e., bFGF).

However, sequential delivery of a second growth factor (e.g., PDGF) can assist with vessel stabilization by recruiting pericytes [62]. Future studies will investigate sequential delivery from ARSs in the HLI model, using previously developed strategies [28, 57, 63, 64].

Conclusions

We have demonstrated that FUS, specifically a mechanism termed ADV, can be used to non-invasively modulate release of bFGF from a fibrin-based ARS. bFGF was initially contained within a phase-shift double emulsion in the ARS. Sustained release of bFGF from the ARS was obtained by applying FUS every three days. FUS-induced release of bFGF yielded significantly greater perfusion in the calf muscle, angiogenesis, and macrophage infiltration compared to other experimental groups. Additionally, less visible ischemia and fibrosis were observed for the ARS+FUS group. Overall, these results highlight the promising therapeutic efficacy of ARSs in conjunction with FUS for stimulating angiogenesis and reperfusion in cardiovascular disease models.

Supplementary Material

Refer to Web version on PubMed Central for supplementary material.

Acknowledgments

This work was supported by NIH Grant R01HL139656 (M.L.F.). H.J. was supported by funds from Guangzhou First People's Hospital of South China University of Technology. Special thanks to Dr. Allen Brooks (Department of Radiology) for assisting with the synthesis of the fluorosurfactant, Aniket Jivani (Department of Radiology) for designing in CAD the holder for the FUS transducer and the FUS exposure platform, and Dr. William Weadock (Department of Radiology) for helping with 3D printing of CAD designs. Additionally, we thank Leidan Huang, Devon Delahoussaye, and Alexander Hostetler for their contributions related to the analysis of histological images.

References

[1]. Fowkes FG, Rudan D, Rudan I, Aboyans V, Denenberg JO, McDermott MM, Norman PE, Sampson UK, Williams LJ, Mensah GA, Criqui MH, Comparison of global estimates of prevalence and risk factors for peripheral artery disease in 2000 and 2010: a systematic review and analysis, Lancet, 382 (2013) 1329–1340. [PubMed: 23915883]

[2]. Soga Y, Takahara M, Iida O, Yamauchi Y, Hirano K, Fukunaga M, Zen K, Suzuki K, Shintani Y, Miyashita Y, Tsuchiya T, Yamaoka T, Ando K, Efficacy of CilostAzol for Below-the-Knee Artery Disease after Balloon AnGioplasty in PatiEnts with Severe Limb Ischemia (CABBAGE Trial), Ann Vasc Surg, 45 (2017) 22–28. [PubMed: 28600024]

[3]. Mustapha JA, Katzen BT, Neville RF, Lookstein RA, Zeller T, Miller LE, Jaff MR, Determinants of Long-Term Outcomes and Costs in the Management of Critical Limb Ischemia: A Population-Based Cohort Study, J Am Heart Assoc, 7 (2018) e009724. [PubMed: 30369325]

[4]. Meloni M, Izzo V, Da Ros V, Morosetti D, Stefanini M, Brocco E, Giurato L, Gandini R, Uccioli L, Characteristics and Outcome for Persons with Diabetic Foot Ulcer and No-Option Critical Limb Ischemia, J Clin Med, 9 (2020).

[5]. Jeon O, Ryu SH, Chung JH, Kim BS, Control of basic fibroblast growth factor release from fibrin gel with heparin and concentrations of fibrinogen and thrombin, Journal of Controlled Release, 105 (2005) 249–259. [PubMed: 16088988]

[6]. Yang HS, Bhang SH, Hwang JW, Kim DI, Kim BS, Delivery of Basic Fibroblast Growth Factor Using Heparin-Conjugated Fibrin for Therapeutic Angiogenesis, Tissue Eng Pt A, 16 (2010) 2113–2119.

[7]. Jeon O, Kang SW, Lim HW, Chung JH, Kim BS, Long-term and zero-order release of basic fibroblast growth factor from heparin-conjugated poly(L-lactide-co-glycolide) nanospheres and fibrin gel, Biomaterials, 27 (2006) 1598–1607. [PubMed: 16146647]

[8]. Lederman RJ, Mendelsohn FO, Anderson RD, Saucedo JF, Tenaglia AN, Hermiller JB, Hillegass WB, Rocha-Singh K, Moon TE, Whitehouse MJ, Annex BH, Investigators T, Therapeutic angiogenesis with recombinant fibroblast growth factor-2 for intermittent claudication (the TRAFFIC study): a randomised trial, Lancet, 359 (2002) 2053–2058. [PubMed: 12086757]

[9]. Ono K, Yanishi K, Ariyoshi M, Kaimoto S, Uchihashi M, Shoji K, Matoba S, First-in-Man Clinical Pilot Study Showing the Safety and Efficacy of Intramuscular Injection of Basic Fibroblast Growth Factor With Atelocollagen Solution for Critical Limb Ischemia, Circulation Journal, 83 (2019) 217-+.

[10]. Cooke JP, Meng S, Vascular Regeneration in Peripheral Artery Disease, Arterioscler Thromb Vasc Biol, 40 (2020) 1627–1634. [PubMed: 32434408]

[11]. Li JY, Mooney DJ, Designing hydrogels for controlled drug delivery, Nat Rev Mater, 1 (2016).

[12]. Mantha S, Pillai S, Khayambashi P, Upadhyay A, Zhang Y, Tao O, Pham HM, Tran SD, Smart Hydrogels in Tissue Engineering and Regenerative Medicine, Materials (Basel), 12 (2019).

[13]. Oliva N, Almquist BD, Spatiotemporal delivery of bioactive molecules for wound healing using stimuli-responsive biomaterials, Advanced drug delivery reviews, 161– (2020) 22–41.

[14]. Yang X, Zhang Y, Yang Y, Lim S, Cao Z, Rak J, Cao Y, Vascular endothelial growth factor-dependent spatiotemporal dual roles of placental growth factor in modulation of angiogenesis and tumor growth, Proceedings of the National Academy of Sciences of the United States of America, 110 (2013) 13932–13937. [PubMed: 23918367]

[15]. Miller DL, Smith NB, Bailey MR, Czarnota GJ, Hynynen K, Makin IRS, Med AIU, Comm B, Overview of Therapeutic Ultrasound Applications and Safety Considerations, J Ultras Med, 31 (2012) 623–634.

[16]. Fabiilli ML, Wilson CG, Padilla F, Martin-Saavedra FM, Fowlkes JB, Franceschi RT, Acoustic droplet-hydrogel composites for spatial and temporal control of growth factor delivery and scaffold stiffness, Acta Biomater, 9 (2013) 7399–7409. [PubMed: 23535233]

[17]. Moncion A, Arlotta KJ, Kripfgans OD, Fowlkes JB, Carson PL, Putnam AJ, Franceschi RT, Fabiilli ML, Design and Characterization of Fibrin-Based Acoustically Responsive Scaffolds for Tissue Engineering Applications, Ultrasound Med Biol, 42 (2016) 257–271. [PubMed: 26526782]

[18]. Janmey PA, Winer JP, Weisel JW, Fibrin gels and their clinical and bioengineering applications, J R Soc Interface, 6 (2009) 1–10. [PubMed: 18801715]

[19]. Whelan D, Caplice NM, Clover AJ, Fibrin as a delivery system in wound healing tissue engineering applications, Journal of controlled release : official journal of theControlled Release Society, 196 (2014) 1–8.

[20]. Riess JG, Understanding the fundamentals of perfluorocarbons and perfluorocarbon emulsions relevant to in vivo oxygen delivery, Artif Cell Blood Sub, 33 (2005) 47–63.

[21]. Kripfgans OD, Fowlkes JB, Miller DL, Eldevik OP, Carson PL, Acoustic droplet vaporization for therapeutic and diagnostic applications, Ultrasound Med Biol, 26 (2000) 1177–1189. [PubMed: 11053753]

[22]. Lacour T, Valier-Brasier T, Coulouvrat F, Ultimate fate of a dynamical bubble/droplet system following acoustic vaporization, Phys Fluids, 32 (2020).

[23]. Duncanson WJ, Arriaga LR, Ung WL, Kopechek JA, Porter TM, Weitz DA, Microfluidic Fabrication of Perfluorohexane-Shelled Double Emulsions for Controlled Loading and Acoustic-Triggered Release of Hydrophilic Agents, Langmuir, 30 (2014) 13765–13770. [PubMed: 25340527]

[24]. Dong X, Lu X, Kingston K, Brewer E, Juliar BA, Kripfgans OD, Fowlkes JB, Franceschi RT, Putnam AJ, Liu Z, Fabiilli ML, Controlled delivery of basic fibroblast growth factor (bFGF) using acoustic droplet vaporization stimulates endothelial network formation, Acta Biomater, 97 (2019) 409–419. [PubMed: 31404713]

[25]. Moncion A, Lin M, O'Neill EG, Franceschi RT, Kripfgans OD, Putnam AJ, Fabiilli ML, Controlled release of basic fibroblast growth factor for angiogenesis using acoustically-responsive scaffolds, Biomaterials, 140 (2017) 26–36. [PubMed: 28624705]

[26]. Lu X, Jin H, Quesada C, Farrell EC, Huang LD, Aliabouzar M, Kripfgans OD, Fowlkes JB, Franceschi RT, Putnam AJ, Fabiilli ML, Spatially-directed cell migration in acoustically-responsive scaffolds through the controlled delivery of basic fibroblast growth factor, Acta Biomater, 113 (2020) 217–227. [PubMed: 32553916]

[27]. Krishna SM, Omer SM, Golledge J, Evaluation of the clinical relevance and limitations of current pre-clinical models of peripheral artery disease, Clin Sci (Lond), 130 (2016) 127–150. [PubMed: 26678170]

[28]. Aliabouzar M, Kripfgans OD, Wang WY, Baker BM, Fowlkes JB, Fabiilli ML, Stable and transient bubble formation in acoustically-responsive scaffolds by acoustic droplet vaporization: theory and application in sequential release, Ultrasonics sonochemistry, in press (2021).

[29]. Lu X, Dong X, Natla S, Kripfgans OD, Fowlkes JB, Wang X, Franceschi R, Putnam AJ, Fabiilli ML, Parametric Study of Acoustic Droplet Vaporization Thresholds and Payload Release From Acoustically-Responsive Scaffolds, Ultrasound Med Biol, 45 (2019) 2471–2484. [PubMed: 31235205]

[30]. Garvin KA, Hocking DC, Dalecki D, Controlling the spatial organization of cells and extracellular matrix proteins in engineered tissues using ultrasound standing wave fields, Ultrasound Med Biol, 36 (2010) 1919–1932. [PubMed: 20870341]

[31]. Anderson EM, Silva EA, Hao Y, Martinick KD, Vermillion SA, Stafford AG, Doherty EG, Wang L, Doherty EJ, Grossman PM, Mooney DJ, VEGF and IGF Delivered from Alginate Hydrogels Promote Stable Perfusion Recovery in Ischemic Hind Limbs of Aged Mice and Young Rabbits, Journal of vascular research, 54 (2017) 288–298. [PubMed: 28930755]

[32]. Patil NS, Dordick JS, Rethwisch DG, Macroporous poly(sucrose acrylate) hydrogel for controlled release of macromolecules, Biomaterials, 17 (1996) 2343–2350. [PubMed: 8982474]

[33]. Aref Z, de Vries MR, Quax PHA, Variations in Surgical Procedures for Inducing Hind Limb Ischemia in Mice and the Impact of These Variations on Neovascularization Assessment, International Journal of Molecular Sciences, 20 (2019).

[34]. Chalothorn D, Zhang H, Clayton JA, Thomas SA, Faber JE, Catecholamines augment collateral vessel growth and angiogenesis in hindlimb ischemia, Am J Physiol Heart Circ Physiol, 289 (2005) H947–959. [PubMed: 15833801]

[35]. Chalothorn D, Faber JE, Strain-dependent variation in collateral circulatory function in mouse hindlimb, Physiol Genomics, 42 (2010) 469–479. [PubMed: 20551146]

[36]. Yang HN, Park JS, Woo DG, Jeon SY, Park KH, Transfection of VEGF(165) genes into endothelial progenitor cells and in vivo imaging using quantum dots in an ischemia hind limb model, Biomaterials, 33 (2012) 8670–8684. [PubMed: 22921925]

[37]. Li Y, Liu W, Liu F, Zeng Y, Zuo S, Feng S, Qi C, Wang B, Yan X, Khademhosseini A, Bai J, Du Y, Primed 3D injectable microniches enabling low-dosage cell therapy for critical limb ischemia, Proceedings of the National Academy of Sciences of the United States of America, 111 (2014) 13511–13516. [PubMed: 25197069]

[38]. McEnaney RM, Shukla A, Madigan MC, Sachdev U, Tzeng E, P2Y2 nucleotide receptor mediates arteriogenesis in a murine model of hind limb ischemia, Journal of vascular surgery, 63 (2016) 216–225. [PubMed: 25088742]

[39]. Arnold L, Henry A, Poron F, Baba-Amer Y, van Rooijen N, Plonquet A, Gherardi RK, Chazaud B, Inflammatory monocytes recruited after skeletal muscle injury switch into antiinflammatory macrophages to support myogenesis, J Exp Med, 204 (2007) 1057–1069. [PubMed: 17485518]

[40]. Huang L, Quesada C, Aliabouzar M, Fowlkes JB, Franceschi RT, Liu Z, Putnam AJ, Fabiilli ML, Spatially-directed angiogenesis using ultrasound-controlled release of basic fibroblast growth factor from acoustically-responsive scaffolds, Acta Biomater, online ahead of print (2021).

[41]. Ozawa CR, Banfi A, Glazer NL, Thurston G, Springer ML, Kraft PE, McDonald DM, Blau HM, Microenvironmental VEGF concentration, not total dose, determines a threshold between normal and aberrant angiogenesis, The Journal of clinical investigation, 113 (2004) 516–527. [PubMed: 14966561]

[42]. Martino MM, Briquez PS, Ranga A, Lutolf MP, Hubbell JA, Heparin-binding domain of fibrin(ogen) binds growth factors and promotes tissue repair when incorporated within a synthetic matrix, Proceedings of the National Academy of Sciences of the United States of America, 110 (2013) 4563–4568. [PubMed: 23487783]

[43]. Andres G, Leali D, Mitola S, Coltrini D, Camozzi M, Corsini M, Belleri M, Hirsch E, Schwendener RA, Christofori G, Alcami A, Presta M, A pro-inflammatory signature mediates FGF2-induced angiogenesis, J Cell Mol Med, 13 (2009) 2083–2108. [PubMed: 18624773]

[44]. Dellacherie MO, Seo BR, Mooney DJ, Macroscale biomaterials strategies for local immunomodulation, Nat Rev Mater, 4 (2019) 379–397.

[45]. Spiller KL, Anfang RR, Spiller KJ, Ng J, Nakazawa KR, Daulton JW, Vunjak-Novakovic G, The role of macrophage phenotype in vascularization of tissue engineering scaffolds, Biomaterials, 35 (2014) 4477–4488. [PubMed: 24589361]

[46]. Troidl C, Jung G, Troidl K, Hoffmann J, Mollmann H, Nef H, Schaper W, Hamm CW, Schmitz-Rixen T, The temporal and spatial distribution of macrophage subpopulations during arteriogenesis, Curr Vasc Pharmacol, 11 (2013) 5–12. [PubMed: 23391417]

[47]. Barzelai S, Sharabani-Yosef O, Holbova R, Castel D, Walden R, Engelberg S, Scheinowitz M, Low-intensity ultrasound induces angiogenesis in rat hind-limb ischemia, Ultrasound Med Biol, 32 (2006) 139–145. [PubMed: 16364805]

[48]. Nazer B, Ghahghaie F, Kashima R, Khokhlova T, Perez C, Crum L, Matula T, Hata A, Therapeutic Ultrasound Promotes Reperfusion and Angiogenesis in a Rat Model of Peripheral Arterial Disease, Circ J, 79 (2015) 2043–2049. [PubMed: 26062950]

[49]. Huang JJ, Shi YQ, Li RL, Hu A, Zhou HS, Cheng Q, Xu Z, Yang ZM, Hao CN, Duan JL, Angiogenesis effect of therapeutic ultrasound on ischemic hind limb in mice, Am J Transl Res, 6 (2014) 703–713. [PubMed: 25628781]

[50]. Burks SR, Ziadloo A, Hancock HA, Chaudhry A, Dean DD, Lewis BK, Frenkel V, Frank JA, Investigation of cellular and molecular responses to pulsed focused ultrasound in a mouse model, PloS one, 6 (2011) e24730. [PubMed: 21931834]

[51]. Helisch A, Wagner S, Khan N, Drinane M, Wolfram S, Heil M, Ziegelhoeffer T, Brandt U, Pearlman JD, Swartz HM, Schaper W, Impact of mouse strain differences in innate hindlimb collateral vasculature, Arterioscl Throm Vas, 26 (2006) 520–526.

[52]. Hellingman AA, Bastiaansen AJNM, de Vries MR, Seghers L, Lijkwan MA, Lowik CW, Hamming JF, Quax PHA, Variations in Surgical Procedures for Hind Limb Ischaemia Mouse Models Result in differences in Collateral Formation, Eur J Vasc Endovasc, 40 (2010) 796–803.

[53]. Jang KW, Tu TW, Nagle ME, Lewis BK, Burks SR, Frank JA, Molecular and histological effects of MR-guided pulsed focused ultrasound to the rat heart, Journal of Translational Medicine, 15 (2017).

[54]. Mac Gabhann F, Peirce SM, Collateral capillary arterialization following arteriolar ligation in murine skeletal muscle, Microcirculation, 17 (2010) 333–347. [PubMed: 20618691]

[55]. Chappell JC, Song J, Burke CW, Klibanov AL, Price RJ, Targeted Delivery of Nanoparticles Bearing Fibroblast Growth Factor-2 by Ultrasonic Microbubble Destruction for Therapeutic Arteriogenesis, Small, 4 (2008) 1769–1777. [PubMed: 18720443]

[56]. Belcik JT, Davidson BP, Xie A, Wu MD, Yadava M, Qi Y, Liang S, Chon CR, Ammi AY, Field J, Harmann L, Chilian WM, Linden J, Lindner JR, Augmentation of Muscle Blood Flow by Ultrasound Cavitation Is Mediated by ATP and Purinergic Signaling, Circulation, 135 (2017) 1240–1252. [PubMed: 28174191]

[57]. Aliabouzar M, Jivani A, Lu XF, Kripfgans OD, Fowlkes JB, Fabiilli ML, Standing wave-assisted acoustic droplet vaporization for single and dual payload release in acoustically-responsive scaffolds, Ultrasonics sonochemistry, 66 (2020).

[58]. Tebebi PA, Kim SJ, Williams RA, Milo B, Frenkel V, Burks SR, Frank JA, Improving the therapeutic efficacy of mesenchymal stromal cells to restore perfusion in critical limb ischemia through pulsed focused ultrasound, Scientific Reports, 7 (2017).

[59]. Lebherz C, von Degenfeld G, Karl A, Pfosser A, Raake P, Pachmayr F, Scholz D, Kupatt C, Boekstegers P, Therapeutic angiogenesis/arteriogenesis in the chronic ischemic rabbit hindlimb:

effect of venous basic fibroblast growth factor retroinfusion, Endothelium, 10 (2003) 257–265. [PubMed: 14660086]

[60]. Bir SC, Fujita M, Marui A, Hirose K, Arai Y, Sakaguchi H, Huang Y, Esaki J, Ikeda T, Tabata Y, Komeda M, New therapeutic approach for impaired arteriogenesis in diabetic mouse hindlimb ischemia, Circ J, 72 (2008) 633–640. [PubMed: 18362437]

[61]. Krishna SM, Omer SM, Li J, Morton SK, Jose RJ, Golledge J, Development of a two-stage limb ischemia model to better simulate human peripheral artery disease, Sci Rep, 10 (2020) 3449. [PubMed: 32103073]

[62]. Cao RH, Brakenhielm E, Pawliuk R, Wariaro D, Post MJ, Wahlberg E, Leboulch P, Cao YH, Angiogenic synergism, vascular stability and improvement of hind-limb ischemia by a combination of PDGF-BB and FGF-2, Nat Med, 9 (2003) 604–613. [PubMed: 12669032]

[63]. Moncion A, Lin M, Kripfgans OD, Franceschi RT, Putnam AJ, Fabiilli ML, Sequential payload release from acoustically-responsive scaffolds uinsg focused ultrasound, Ultrasound Med Biol, 44 (2018) 2323–2335. [PubMed: 30077413]

[64]. Aliabouzar M, Kripfgans OD, Wang WY, Baker BM, Fowlkes JB, Fabiilli ML, Stable and transient bubble formation in acoustically-responsive scaffolds by acoustic droplet vaporization: theory and application in sequential release, Ultrasonics sonochemistry, in press (2020).

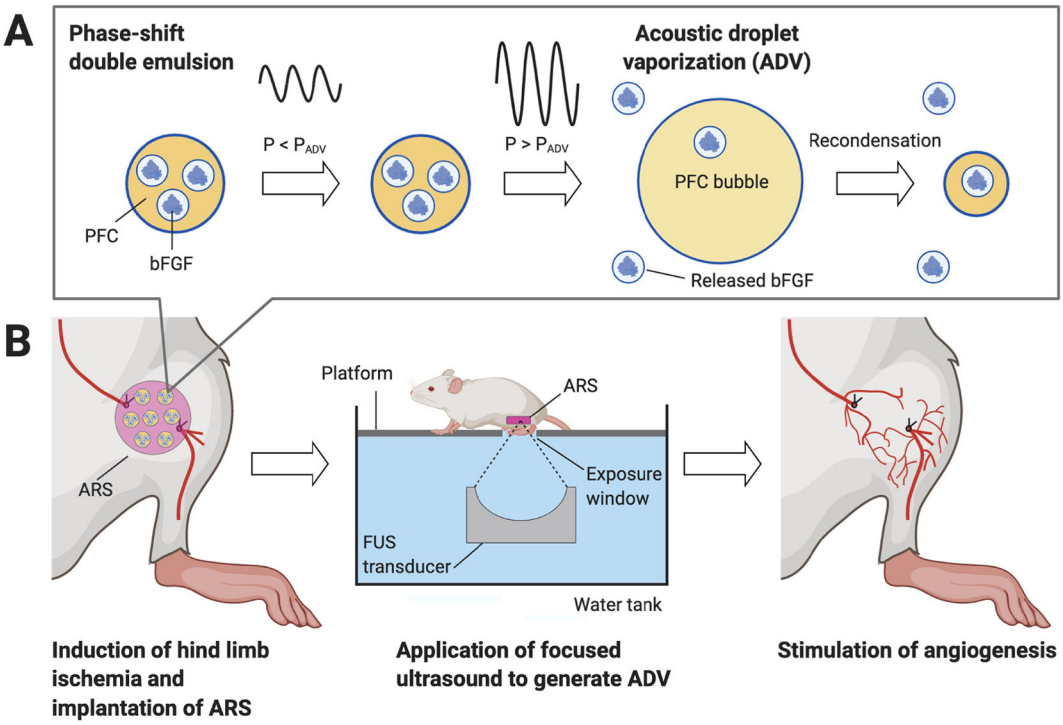

Figure 1.

Focused ultrasound (FUS) was used to control release of basic fibroblast growth factor (bFGF) from an acoustically-responsive scaffold (ARS). The ARS consists of a fibrin matrix doped with a phase-shift double emulsion containing bFGF. The FUS-based release mechanism is termed acoustic droplet vaporization (ADV). A) At subthreshold acoustic pressures (i.e., $P < P_{ADV}$), the perfluorocarbon (PFC) phase within the emulsion remains a liquid. At suprathreshold pressures (i.e., $P > P_{ADV}$), the PFC phase is vaporized into a bubble, thereby causing release of the encapsulated bFGF. Due to its high bulk boiling point, the PFC used in this study ultimately recondenses [28]. B) An ARS was implanted at the site of femoral artery resection in mice. Suprathreshold FUS was transcutaneously applied to release bFGF, which subsequently stimulated angiogenesis and reperfusion. The figure was created with BioRender.com.

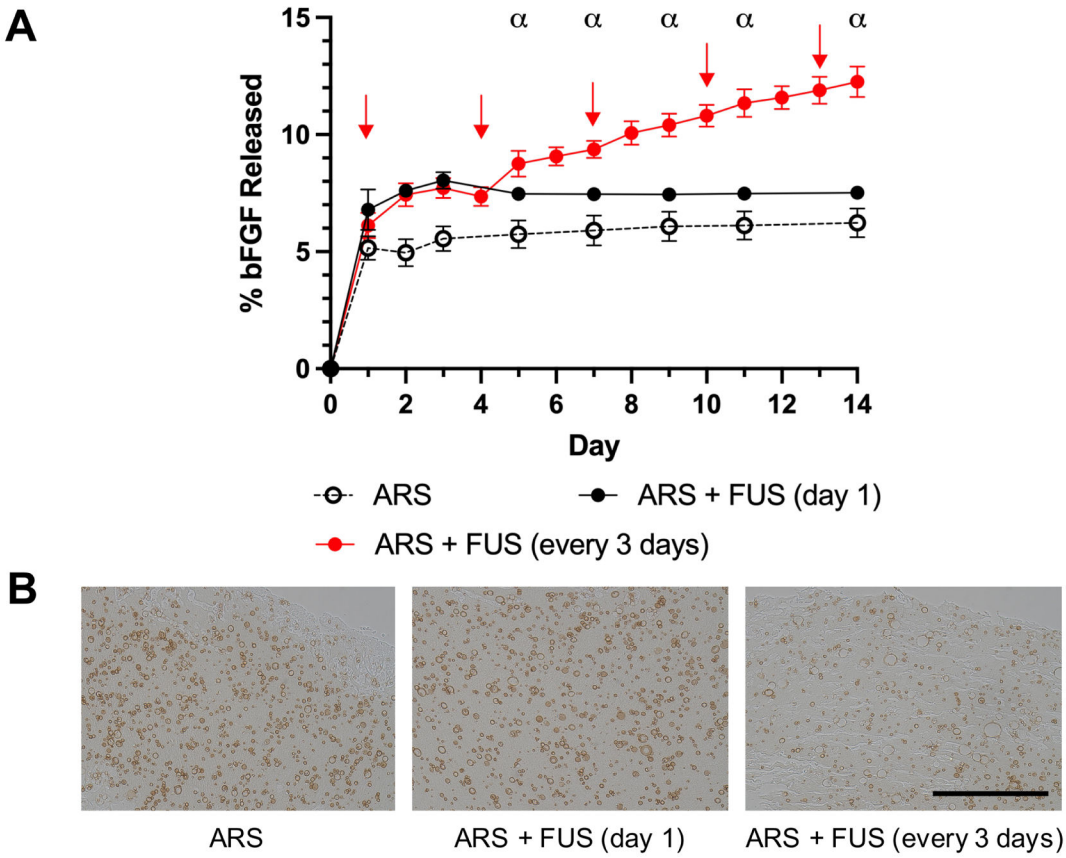

Figure 2.

In vitro release of bFGF from ARSs correlated with the number of suprathreshold FUS exposures. A) On day 1, ARSs containing 3.3% (v/v) bFGF-loaded, phase-shift emulsion were exposed to FUS either once or every three days (denoted by red arrows). Data are represented as mean ± standard deviation (N=5 per group). Statistically significant differences ($p < 0.01$) are denoted as follows. α: ARS + FUS (day 1) vs. ARS + FUS (every 3 days). B) ARSs were immunohistochemically stained for bFGF. Brightfield images reveal morphological differences caused by FUS-induced vaporization of the phase-shift emulsion. Scale bar: 200 μm.

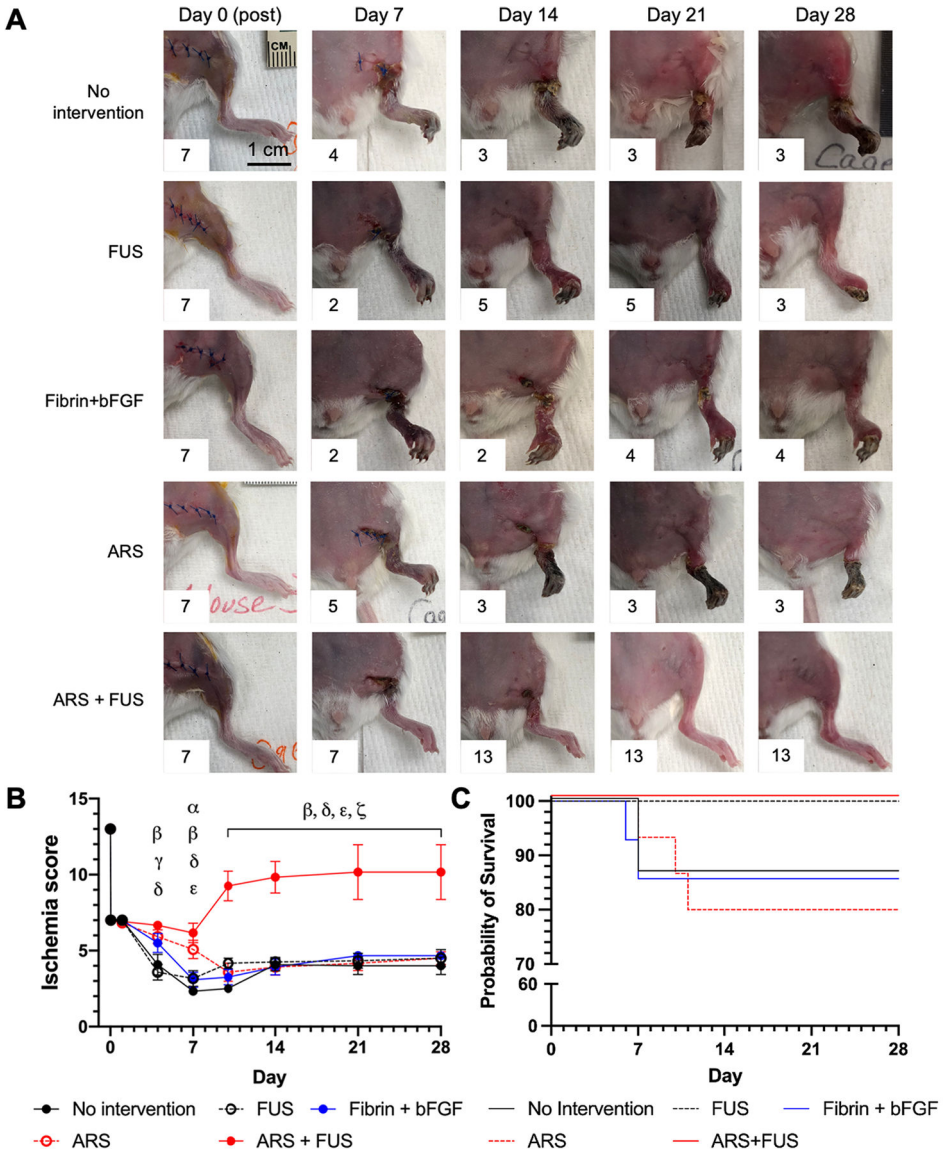

Figure 3.

The greatest therapeutic efficacy, as evaluated visually based on the level of discoloration and/or necrosis in the left leg, was observed in mice that received ARSs in conjunction with FUS applied every three days (i.e., ARS + FUS). A) Representative, longitudinal images of mice from the five experimental groups are shown. The ischemia score for each image is displayed as an inset. B) The level of ischemia was quantitatively scored across the 28 day study. The ischemia score is inversely related to the amount of ischemia, with a score of 13 assigned to a healthy leg prior to surgery. Data are represented as mean ± standard error of the mean (N=12–13 per group for days 0–14 and N=6 for days 21–28). Statistically significant differences ($p < 0.05$) are denoted as follows. α: no intervention vs. ARS; β: no intervention vs. ARS + FUS; γ: FUS vs. ARS; δ: FUS vs. ARS + FUS; ε: fibrin + bFGF vs. ARS + FUS; and ζ: ARS vs. ARS + FUS. C) Kaplan-Meier curves are shown for the five

experimental groups. Mice that displayed necrosis exceeding the approved endpoint were euthanized, which occurred between days 6 and 11 of the study.

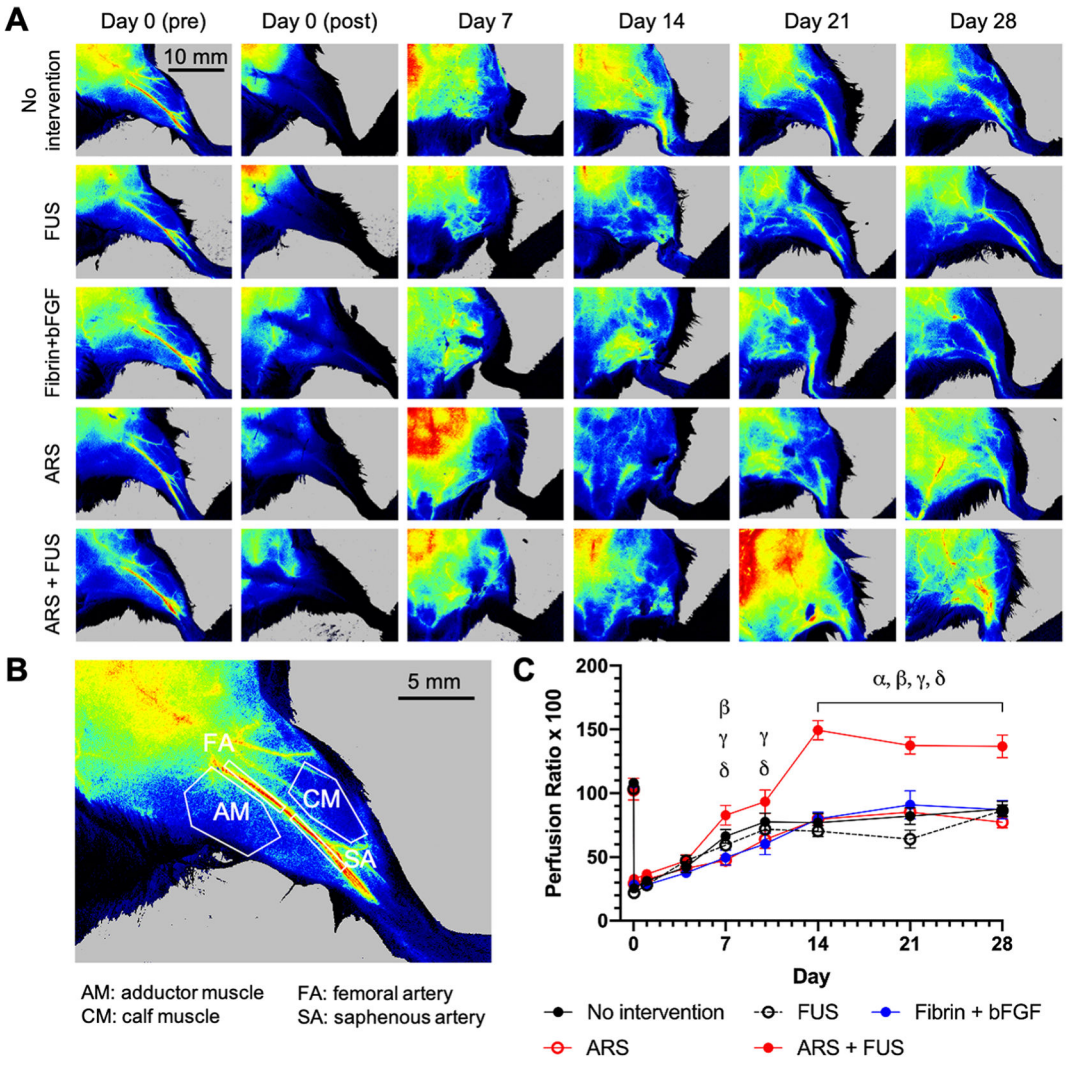

Figure 4.

Perfusion was longitudinally tracked using laser speckle contrast analysis (LASCA) imaging. A) Representative, longitudinal images of mice from the five experimental groups are shown. B) Perfusion was assessed in four different regions of interest (ROIs) within the leg as well as in the foot (not shown). This image shows a leg prior to surgery. C) For each ROI, a perfusion ratio was calculated by normalizing the average relative perfusion in the ischemic limb by the normal limb. The longitudinal profiles for the calf muscle ROI are shown. Data are represented as mean ± standard error of the mean (N=12–13 per group for days 0–14 and N=6 for days 21–28). Statistically significant differences ($p < 0.05$) are denoted as follows. α: no intervention vs. ARS +FUS; β: FUS vs. ARS + FUS; γ: fibrin + bFGF vs. ARS + FUS; and δ: ARS vs. ARS + FUS.

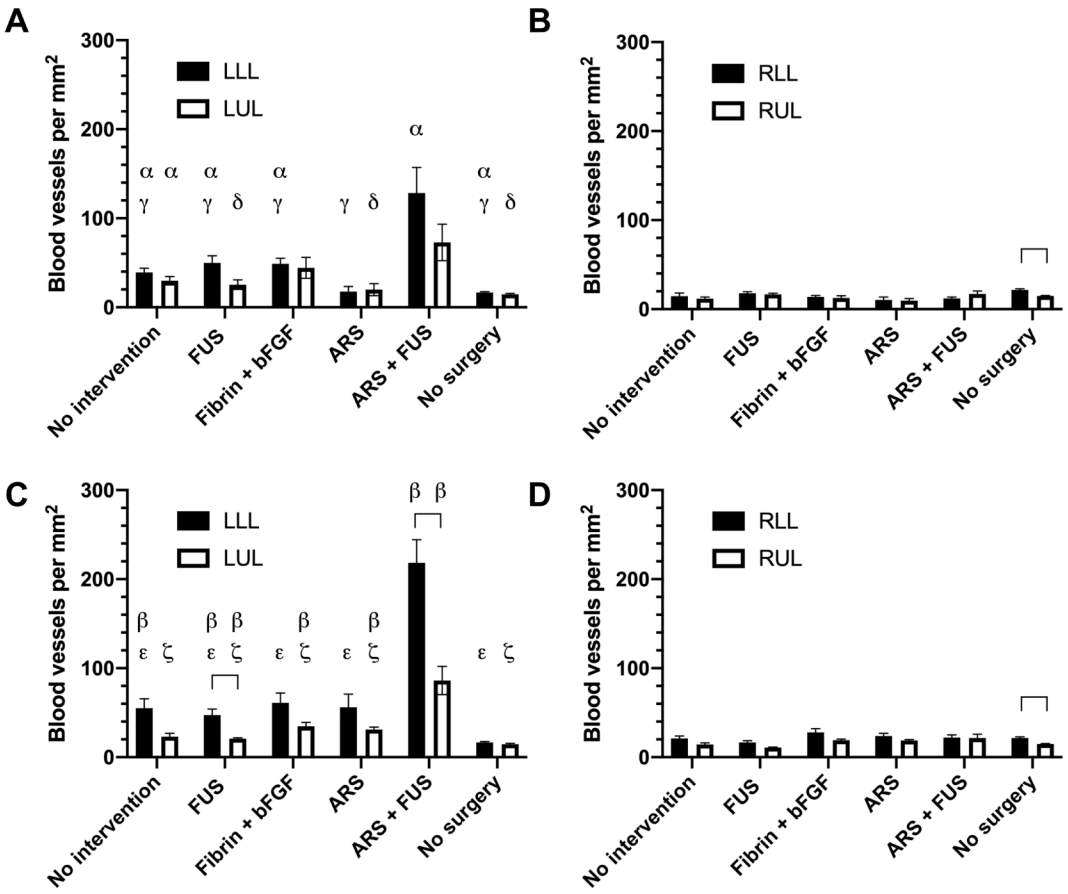

Figure 5.

The density of blood vessels was assessed using CD31 immunohistochemistry on day 14 (A, B) and day 28 (C, D) within the left (i.e., ischemic) as well as right (i.e., normal) legs. Four different regions of muscle were analyzed: left lower leg (LLL), left upper leg (LUL), right lower leg (RLL), and right upper leg (RUL). All groups underwent HLI surgery except for the 'no surgery' group. Data are represented as mean ± standard error of the mean (N=6–7 per group for day 14, N=6 for day 28, and N=4 for the 'no surgery' group). Statistically significant differences ($p < 0.05$) are denoted by brackets as well as the following symbols. α: LLL at day 14 vs. RLL at day 14; β: LLL at day 28 vs. RLL at day 28; γ: vs. ARS + FUS (LLL at day 14); δ: vs. ARS + FUS (LUL at day 14); ε: vs. ARS + FUS (LLL at day 28); and ζ: vs. ARS + FUS (LUL at day 28).

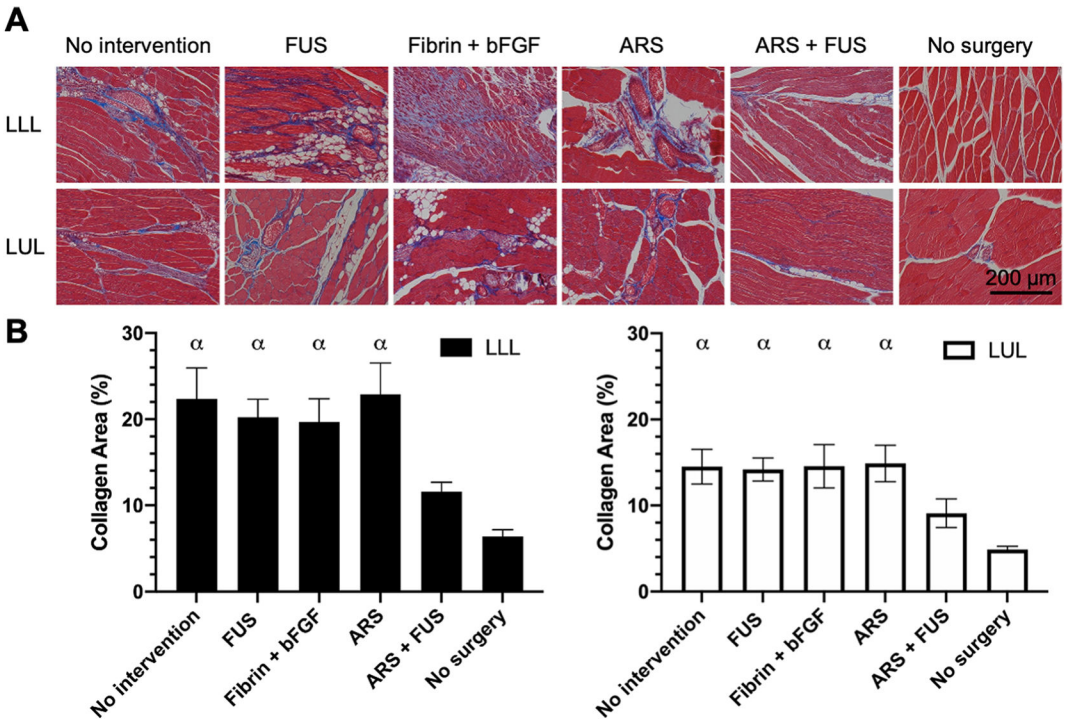

Figure 6.

Fibrosis was evaluated based on Masson's trichrome staining. A) Representative images are shown from the left lower leg (LLL) and left upper leg (LUL) from the experimental groups on day 28 as well as control mice (i.e., 'no surgery'). B) The area percent of each image that stained positive for collagen (i.e., blue) was quantified. Data are represented as mean ± standard error of the mean (N=6 for each experimental group and N=4 for the 'no surgery' group). Statistically significant differences ($p < 0.05$) are denoted as follows. α: vs. no surgery.

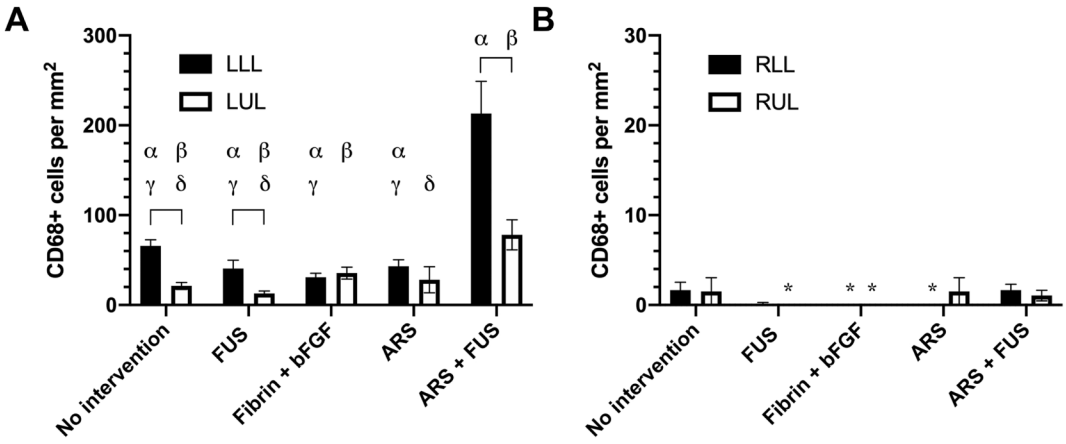

Figure 7.

The density of macrophages was assessed using CD68 immunohistochemistry on day 28 within the left (A) and right legs (B). Four different regions of muscle were analyzed: left lower leg (LLL), left upper leg (LUL), right lower leg (RLL), and right upper leg (RUL). Data are represented as mean ± standard error of the mean (N=6 per group). An asterisk (*) denotes each group where zero CD68+ cells were counted. Statistically significant differences ($p < 0.05$) are denoted by brackets as well as the following symbols. α: LLL vs RLL; β: LUL vs. RUL; γ: vs. ARS + FUS (LLL); and δ: vs. ARS + FUS (LUL).